KSCE Journal of Civil Engineering
DOI 10.1007/s12205-024-1566-6

pISSN 1226-7988, eISSN 1976-3808
www.springer.com/12205

Structural Engineering

Steel-Concrete Bond versus Primary Crack Opening in Reinforced Concrete Beams

Jianming Wang[a], **Jian Guo**[a], **and Chunyu Fu**[b]

[a]*Dept. of Bridge Engineering, Southwest Jiaotong University, Chengdu 610031, China*
[b]*Dept. of Civil and Transportation Engineering, Hohai University, Nanjing 210098, China*

ARTICLE HISTORY

Received 1 August 2023
Revised 1 April 2024
Accepted 27 May 2024
Published Online 23 July 2024

KEYWORDS

RC beams
Crack opening
Primary cracks
Bar–concrete bond
Bond stress-slip relationship
Nonlinear structural behavior

ABSTRACT

Bond deterioration between steel bars and concrete in reinforced-concrete beams mostly occurs close to the primary (i.e., bending induced) cracks. To investigate bond-cracking interaction, a novel bond-slip relationship is introduced in this study, where bond parameters are a function of crack-opening displacement. Such a displacement is in turn evaluated based on the highly variable strain profiles in the concrete, through an iterative procedure. The effectiveness of the proposed approach is validated against a set of tests on RC beams well-documented in the literature, which show a clear trend for the local bond stresses to decrease close to the primary cracks. The bond-slip relationships along the bar and the maximum bond stress depend on the applied loads and on the crack pattern, with a mutual interaction that affects both the crack-opening displacement and the bond stresses, causing a nonlinear increase in the steel strains. Nevertheless, the bond-slip relationships display descending branches characterized by remarkably similar slopes within a given region, irrespective of the loads. Consequently, if the descending branch for this region is known under a particular load, the branches under other loads can be obtained by horizontally translating the known branch. The proposed approach may provide a useful tool to describe bond behavior in RC members and to understand the complex interaction among the displacements due to crack opening, bond stresses and their structural effect.

1. Introduction

Bond performance between steel bars and concrete is an important property of reinforced concrete (RC) structures, which is highly relevant at the serviceability limit state by governing the crack behavior and deformation capacity of RC structures (Fib, 2014). Over time the bond may deteriorate due to bar and concrete degradation (Fib, 2000). If concrete cracks occur in regions surrounding the bars, some of the bar-concrete interfaces are destroyed, and the bond stresses are greatly weakened (Cairns and Jones, 1996; Gambarova and Rosati, 1997; Giuriani and Plizzari, 1998; Kaklauskas, 2017). Especially at the crack locations, the loss of contact between bar and concrete leads to a bond stress of zero (Wu and Gilbert, 2009). Therefore, it is essential to analyze the bond performance in the cracked RC structures.

Several models have been proposed to represent the bond-slip relationship for cracked structures. Early linear models assumed a constant bond stress over the bonded length to predict the process of crack propagation or the deflection of cracked beams (Ruiz, 2001; Parvanova and Gospodinov, 2008; Castel et al., 2012), whereas nonlinear models explored piecewise linear or curvilinear relationships to analyze the effect of tension stiffening and cyclic behavior (Marfia et al., 2004; Rabczuk et al., 2005; Yankelevsky et al., 2008). However, these models have often relied on the bond-slip relationship derived from pull-out tests conducted on short specimens, neglecting the presence of cracks. This oversight has resulted in incomplete characterization of bond behavior.

Intense deterioration of bond occurs wherever the bars cross a primary bending-induced crack, followed by the formation of secondary microcracks or splitting cracks (Gambarova et al., 1989; Cairns and Jones, 1996; Jakubovskis and Kaklauskas, 2019). Various researchers have proposed approaches to incorporate the effect of secondary microcracks on bond behavior, considering

CORRESPONDENCE Chunyu Fu fuyupiece@163.com Dept. of Civil and Transportation Engineering, Hohai University, Nanjing 210098, China

factors like a damage variable or stiffness reduction (Ruiz et al., 2007; Debernard et al., 2013; Castel et al., 2014; Debernard and Taliano, 2016; Taliano, 2017; Xu et al., 2018; Tan et al., 2020; Jakubovskis and Kaklauskas, 2021; Somma et al., 2021). To account for bond deterioration associated with splitting cracks, the bond-slip relationship has been adjusted as a function of splitting widths (Gambarova and Rosati, 1997; Mousavi et al., 2019; Hermawan et al., 2023). However, the mechanical behavior ensuing from the opening of the primary cracks is often neglected, despite their significant influence on bond deterioration (Murray et al., 2018).

In practice, the bond stress-slip in RC beams undergoes deterioration even in the absence of microcracks. This deterioration occurs in the regions closest to the primary cracks, causing the concrete to break at the crack interfaces. Consequently, the bond stresses vanish at these interfaces. However, the slip values between the bars and concrete gradually increase, reaching their maximum values close to these interfaces. This phenomenon results in a descending pattern in the bond stress-slip relationship, indicating bond deterioration. To effectively capture this deterioration, a novel model was proposed, whose parameters are a function of the slip at the interface with a primary crack and not only of material properties (Fu and Lao, 2023). This model has proven to be accurate in predicting the bond stresses of RC tension members with primary cracks.

In this study, the mechanical behavior of the bond in RC beams exhibiting primary cracks is investigated. To achieve this, a bond stress-slip model, whose parameters are function of the crack-opening displacement of the primary cracks, is introduced. The relationship requires the formulation of an accurate model to describe bond behavior in RC cracked beams and specifically the nonlinear strains in the concrete embedment. The formulation of this model is accomplished through an iterative process. The proposed approach will, hopefully, improve the understanding of bond behavior in RC beams and bond-related structural effects.

2. Bar-Concrete Bond Model

In this study, an RC beam with primary cracks is investigated. When subjected to external loads, a slip occurs between the steel bar and concrete, reaching its local maximum values at the crack interfaces. However, the bond force between the bar and concrete diminishes to 0 at these interfaces (Cantone et al., 2021). Consequently, the bond force-slip relationship exhibits a descending pattern near the cracks. To address this behavior, a bond force-slip relationship that depends on the slip at the interfaces was proposed (Fu and Lao, 2023):

$$f_b = f_{b0}\left(1 - \frac{s}{s_{cc}}\right), \tag{1}$$

where s denotes the slip between the steel bar and the surrounding concrete, f_b denotes the bond force per unit length, f_{b0} is a constant, and s_{cc} is the slip at the interface of the studied crack.

At the crack interface, the concrete undergoes fracture, whereas

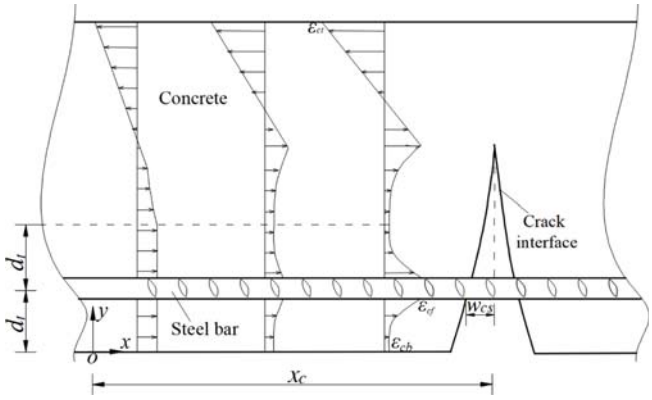

Fig. 1. Concrete Strain Variation Near a Primary Crack

the bar keeps its integrity. Crack opening results from the lack of compatibility between the displacement in the bar and that in the surrounding concrete, because of the different deformation capabilities of the two materials. Hence a slip occurs at the interface (Balazs, 1993; Giuriani and Plizzari, 1998). As a result, the slip s_{cc} at the interface tends to coincide with one half w_{cs} of the crack-opening displacement w_{ct}, as shown in Fig. 1. This relationship allows for the reformulation of Eq. (1) as follows:

$$\tau = \tau_{b0}\left(1 - \frac{s}{w_{cs}}\right), \tag{2}$$

where τ is the bond stress, and τ_{b0} is a constant.

For a greater distance from the crack, the influence of the cracks on the bond diminishes, and the slip values become small. The ascending part of the relationship given by the fib Model Code (Fib, 2013) is adopted to describe τ:

$$\tau(s) = \tau_{\max}\left(\frac{s}{s_{sm}}\right)^{0.4}, \tag{3}$$

where $\tau_{\max}$ represents the maximum bond stress achieved during pull-out tests, and s_{sm} denotes the slip corresponding to the occurrence of $\tau_{\max}$. Both $\tau_{\max}$ and s_{sm} are experimentally determined

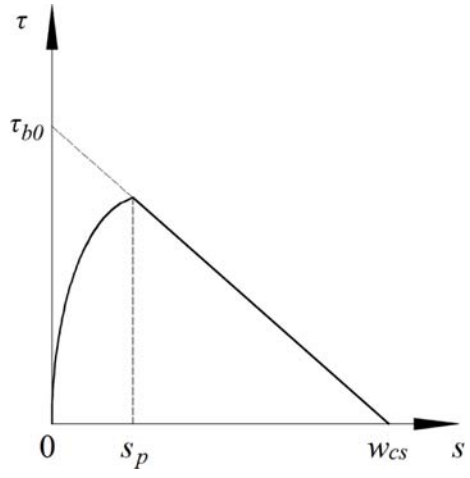

Fig. 2. Relationship between the Bond Force and Slip

and take care of the bond properties between the bar and concrete.

Therefore, the bond stress-slip relationship in the region between the primary cracks is represented as a piecewise function, as shown in Fig. 2. The curved and linear branches depict bond behavior in the regions beside the cracks (where the bar-concrete interface is mostly undamaged) and astride the cracks (where the bond stress goes to zero in the mean plane of the crack), respectively. Therefore, the curved branch indicates the activation of bond far from the primary cracks, where the steel strain and the average concrete strain coincide, while the linear branch indicates the vanishing of bond from the crack interfaces.

The bond stresses reach their local peak at the intersection of the curved and linear branches, where the slip is denoted as s_p. Since s_p corresponds to the local peak stress between the cracks under a specific load, which is typically lower than the maximum bond stresses observed during pull-out tests, s_p is inherently smaller than s_{sm}.

For any given infinitesimal portion of the bar-concrete system, the slip ds is the difference between the elongation of the bar and the average elongation of the surrounding concrete over the length dx of the portion in question:

$$\mathrm{d}s = (\varepsilon_s - \varepsilon_c)\mathrm{d}x\,, \tag{4}$$

where ε_c and ε_s denote the concrete and steel strains, respectively. The relationships between the strains and bond stress over the length can be expressed as:

$$E_s A_s \frac{\mathrm{d}\varepsilon_s}{\mathrm{d}x} = \tau L_s\,, \tag{5}$$

$$E_c A_{ef} \frac{\mathrm{d}\varepsilon_c}{\mathrm{d}x} = -\tau L_s\,, \tag{6}$$

where A_s and A_{ef} are the effective areas of the steel bar and concrete, respectively; E_s and E_c denote the elastic moduli of the steel bar and concrete, respectively; L_s denotes the contact perimeter of the steel bar.

Near the interfaces of primary cracks, the concrete strains exhibit significant nonlinearities in the sections, and the bond force acting upon the concrete occurs over a region much smaller than the dimensions of the concrete transverse section (Murray et al., 2018), as shown in Fig. 1. The region subjected to bond forces was defined as an effective tensile section characterized by homogenized average bond stresses, with its effective area assumed to vary with the slip (Fu and Lao, 2023):

$$A_{ef} = \frac{2A_{c0}w_{cs}}{\alpha_0}\left(1 - \frac{s}{w_{cs}}\right), \tag{7}$$

where α_0 is a constant, and A_{c0} is the actual concrete area. Previous studies have indicated that the strain profile in the region with a height of $2d_t$ is affected by the bond stresses for the beams (Fib, 2013), leading to A_{c0} being equal to $2bd_t$, where b is the width of the beam section and d_t is the distance from the steel bar to the bottom.

To obtain the general differential equation governing bond problem in an anchored bar or in a tension tie, Eqs. (5) and (6) should be implemented into the derivative of Eq. (4) (Fayyad and Lees, 2018):

$$\frac{\mathrm{d}^2 s}{\mathrm{d}x^2} = \tau L_s\left(\frac{1}{E_s A_s} + \frac{1}{E_c A_{ef}}\right). \tag{8}$$

As the bond stress is expressed using two piecewise functions (Eqs. (2) and (3)), a step strategy is used to solve Eq. (8). First, the linear branch of the bond stress-slip relationship is adopted and (8) is rewritten as follows, by substituting Eqs. (2) and (7) into it:

$$\frac{\mathrm{d}^2 s}{\mathrm{d}x^2} + \beta_1^2 s = \beta_1^2 s_{c0}\,, \tag{9}$$

where β_1 is a calculated coefficient, and s_{c0} is an equivalent slip. β_1 and s_{c0} can be expressed as

$$\beta_1 = \sqrt{\frac{\tau_{b0} L_s}{E_s A_s w_{cs}}}\,, \tag{10}$$

$$s_{c0} = w_{cs} + \frac{\alpha_0 E_s A_s}{4E_c b d_t}\,. \tag{11}$$

Subsequently, the curved branch of the relationship is adopted. Eq. (3) is substituted into Eqs. (8), and Eq. (8) is rewritten as:

$$\frac{\mathrm{d}^2 s}{\mathrm{d}x^2} - s^{0.4}\beta_2 = 0\,, \tag{12}$$

where β_2 is a calculated coefficient and can be expressed as

$$\beta_2 = \frac{\tau_{\max} L_s}{s_{sm}^{0.4}}\left(\frac{1}{E_s A_s} + \frac{1}{2E_c b d_t}\right). \tag{13}$$

To solve these equations, the origin of the coordinate system is assumed to be positioned in the mid-section between two contiguous cracks. While the bond stress is represented by the piecewise function, the bond stress and slip are treated as smooth and continuous at the intersection, which can be expressed as:

$$\tau\big|_{x = x_p - \delta x} = \tau\big|_{x = x_p + \delta x}\,, \tag{14}$$

$$\left.\frac{\mathrm{d}s}{\mathrm{d}x}\right|_{x = x_p - \delta x} = \left.\frac{\mathrm{d}s}{\mathrm{d}x}\right|_{x = x_p + \delta x}\,, \tag{15}$$

where δx denotes a positive infinitesimal value, and x_p is the coordinate of the intersection.

Based on these boundary conditions at the cracks, coordinate origin, and intersection, the solution for Eq. (9) can be obtained (Fu and Lao, 2023):

$$s(x) = -\frac{\varepsilon_{sc}}{\beta_1}\sin\beta_1\left(x_c - x\right) + w_{cs}\,, \tag{16}$$

where ε_{sc} represents the steel strain at the cracked section, and x_c denotes the x-axis coordinate of the crack, indicating the distance

from the crack to the origin of the coordinate system, with its unit in meters. As illustrated in Fig. 1, the absolute value of x_c is likely equal to half of the crack spacing. The approximate solution for Eq. (12) can be expressed as (Muhamad et al., 2012):

$$s(x) = \sqrt{2c_3 x}\,, \tag{17}$$

$$c_3 = \frac{\varepsilon_{sc}^2 \cos^2\beta_1 (x_c - x_p)}{2} - \frac{\beta_2 s_p^{1.4}}{1.4}\,. \tag{18}$$

The constants are also solved:

$$\alpha_0 = 2(s_{cc} - s_p)\,, \tag{19}$$

$$\tau_{b0} = \frac{\tau_{\max} w_{cs} s_p^{0.4}}{(w_{cs} - s_p) s_{sm}^{0.4}}\,, \tag{20}$$

$$x_p = x_c - \frac{1}{\beta_1} \arcsin\left[\frac{\beta_1 (w_{cs} - s_p)}{\varepsilon_{sc}}\right]. \tag{21}$$

For $x > x_p$, steel and concrete strains can be evaluated by combining Eqs. (2), (5), (6), (16) and (20).

$$\varepsilon_s = \varepsilon_{sc} - \frac{\tau_{\max} L_s \varepsilon_{sc} s_p^{0.4}}{(w_{cs} - s_p) E_s A_s \beta_1^2 s_{sm}^{0.4}} \left\{1 - \left[\cos\beta_1 (x_c - x)\right]\right\}, \tag{22}$$

$$\varepsilon_{cf} = \frac{\tau_{\max} L_s s_p^{0.4}}{2 E_c b d_t s_{sm}^{0.4}} (x_c - x)\,. \tag{23}$$

Based on Eqs. (22) and (23), the steel and concrete strains at x_p, denoted as ε_{sp} and ε_{cfp}, respectively, can be obtained.

$$\varepsilon_{sp} = \varepsilon_{sc} - \frac{\tau_{\max} L_s \varepsilon_{sc} s_p^{0.4}}{(w_{cs} - s_p) E_s A_s \beta_1^2 s_{sm}^{0.4}} \left\{1 - \left[\cos\beta_1 (x_c - x_p)\right]\right\}, \tag{24}$$

$$\varepsilon_{cfp} = \frac{\tau_{\max} L_s s_p^{0.4}}{2 E_c b d_t s_{sm}^{0.4}} (x_c - x_p)\,. \tag{25}$$

For $x \le x_p$, steel and concrete strains can be evaluated by combining Eqs. (2), (5), (6), (17) and (20).

$$\varepsilon_s = \varepsilon_{sp} - \frac{\tau_{\max} L_s (2c_3)^{0.2} (x_p - x)^{1.4}}{1.4 E_s A_s s_{sm}^{0.4}}\,, \tag{26}$$

$$\varepsilon_{cf} = \varepsilon_{cfp} + \frac{\tau_{\max} L_s (2c_3)^{0.2} (x_p - x)^{1.4}}{2.8 E_c b d_t s_{sm}^{0.4}}\,. \tag{27}$$

By using these strains, s_{cc} and s_p are calculated:

$$s_{cc} = \int_0^{x_c} (\varepsilon_s - \varepsilon_{cf})\mathrm{d}x = \varepsilon_{sc} x_c - \frac{\tau_{\max} L_s (2c_3)^{0.2}}{3.36 s_{sm}^{0.4}} \left(\frac{1}{E_s A_s} + \frac{1}{2E_c b d_t}\right) x_p^{2.4} - \frac{\tau_{\max} L_s s_p^{0.4}}{4E_c b d_t s_{sm}^{0.4}} (x_c^2 - x_p^2) + \frac{\tau_{\max} L_s \varepsilon_{sc} s_p^{0.4}}{(w_{cs} - s_p) E_s A_s \beta_1^2 s_m^{0.4}} \left[\frac{\sin\beta_1 (x_c - s_p)}{\beta_1} - x_c + x_p \cos\beta_1 (x_c - x_p)\right], \tag{28}$$

$$s_p = s_{ss} - \int_{x_p}^{x_c} (\varepsilon_s - \varepsilon_c)\mathrm{d}x = s_{cc} - \varepsilon_{sc}(x_c - x_p) + \frac{\tau_{\max} L_s s_p^{0.4}}{2E_c A_{c0} s_{sc}^{0.4}} (x_c - x_p)^2 + \frac{\tau_{\max} L_s \varepsilon_{sc} s_p^{0.4}}{(s_{cc} - s_p) E_s A_s \beta_1^2 s_{sc}^{0.4}} \left[x_c - s_p + \frac{\sin\beta_1 (x_c - x_p)}{\beta_1}\right]. \tag{29}$$

If s_{cc} is known, the steel strain ε_{sc} at the crack can be calculated by rewriting Eq. (28).

$$\varepsilon_{sc} = \frac{s_{cc} + \frac{\tau_{\max} L_s (2c_3)^{0.2}}{3.36 s_{sm}^{0.4}} \left(\frac{1}{E_s A_s} + \frac{1}{E_c A_{c0}}\right) x_p^{2.4} + \frac{\tau_{\max} L_s s_p^{0.4}}{2E_c A_{c0} s_{sm}^{0.4}} (x_c^2 - x_p^2)}{x_c + \frac{\tau_{\max} L_s s_p^{0.4}}{(s_{cc} - s_p) E_s A_s \beta_1^2 s_{sm}^{0.4}} \left[\frac{\sin\beta_1 (x_c - x_p)}{\beta_1} - x_c + x_p \cos\beta_1 (x_c - x_p)\right]} \tag{30}$$

3. Nonlinear Bond Behavior

3.1 Strain Profiles in the Transverse Sections Close to the Primary Cracks

The analysis of bond behavior presented above is dependent on the bond stress-slip relationship governed by the crack-opening displacement, as shown in Eq. (2). Since the displacement ensues from beam's deformations, it is intrinsically linked to the strain profiles near the primary crack. Hence, a comprehensive investigation of these strain profiles is necessary to understand their influence on the crack-opening displacement and, ultimately, on the overall bond behavior of RC beams.

In addition to the region near the bars, concrete tensile strains also occur near the crack tip, and the profile of these strains exhibits sizeable nonlinearities in the transverse sections due to stress concentration at the tip. To describe this strain profile, a nonlinear model is proposed, as depicted in Fig. 1. It is assumed that an inflection point appears at a depth that is the same as the crack tip, and two different profiles occur above and below the crack tip, respectively (Fu et al., 2022). The concrete strains above the tip remain linear along the section depth, whereas the strains below the tip follow a nonlinear profile, which is simulated by a polynomial profile.

$$\varepsilon_c(y) = \left(\varepsilon_{ct} \frac{d_c - y_n}{h - y_n} - \varepsilon_{cb}\right)\left(\frac{y - 2d_t}{d_c}\right)^3 + \varepsilon_{cb} \quad 2d_t \le y \le d_c\,, \tag{31}$$

where ε_{cb} and ε_{ct} are the bottom and top strains, respectively, h is the beam depth, d_c is the crack depth, and y_n is the y axis coordinate of the section neutral axis.

To determine the strain profile, the top strain and neutral axis of the section should be evaluated using internal force equilibrium for the studied beam:

$$\int_{A_{ca}} E_c \varepsilon_c(y) dA + E_t \varepsilon_t A_t + E_c \varepsilon_{cf} A_{ef} = 0\,, \tag{32}$$

$$\int_{A_{ca}} E_c \varepsilon_c(y)(y - y_n) dA + E_t \varepsilon_t A_t (d_t - y_n) + E_c \varepsilon_{cf} A_{ef} (d_t - y_n) = M_0\,, \tag{33}$$

where M_0 denotes the bending moment acting on the section, and

A_{ca} is the area of the concrete above the region affected by the bond stress. Once the steel strains are known, ε_{ct} and y_n can be calculated based on Eqs. (32) and (33).

3.2 Solving Process

If the crack interface is planar, as shown in Fig. 1, the crack-opening displacement w_{cs} can be expressed as:

$$w_{cs} = \frac{w_{cb}}{d_c}(d_c - d_t), \tag{34}$$

where w_{cb} denotes the crack-opening displacement at the bottom of the beam. w_{cb} can be taken as the difference between the elongation of the bottom and the sum of the concrete strains at the bottom, which is written as

$$w_{cb} = \Delta l_{ce} - \Delta l_{cd}, \tag{35}$$

where Δl_{ce} is the bottom elongation, and Δl_{cd} denotes the strain sum:

$$\Delta l_{cd} = \int_0^{l_t} \varepsilon_{cb}(x)dx. \tag{36}$$

In spite of the high nonlinearity of the strains in the concrete section, a linear profile from the top of the section to the neutral axis may still be assumed (Fig. 1). Consequently, when calculating the deformation capacity of the cracked beam, it is viable to treat the beam as one adhering to the plane-section hypothesis (Fu et al., 2021). In this context, the equivalent inertia I_{eq} of transverse sections can be expressed using the top strain and neutral axis,

$$I_{eq} = \frac{M_0}{E_c \varepsilon_{ct}}(h - y_n). \tag{37}$$

Based on this inertia, the elongation of the beam bottom can be expressed as

$$\Delta l_{ce} = \int_0^{l_t} \frac{M_0}{I_{eq} E_c} y_n \mathrm{d}x. \tag{38}$$

Substituting Eqs. (37) into (38), the elongation is rewritten as

$$\Delta l_{ce} = \int_0^{l_t} \frac{\varepsilon_{ct} y_n}{(h - y_n)} \mathrm{d}x. \tag{39}$$

By substituting Eqs. (39) and (36) into Eq. (35), the crack-opening displacement w_{cb} can be evaluated, while Eq. (34) makes it possible to evaluate the crack-opening displacement w_{cs} and the slip s_{cc} in the cracked plane. These evaluated results are then used to recalculate the steel strain ε_{sc} at the crack and the slip s_p using Eqs. (29) and (30), respectively.

Given that w_{cs} and s_p are pivotal parameters in the bond stress-slip relationship, as illustrated in Fig. 2, it is imperative to update the relationship once these parameters are recalculated based on the crack-opening displacement results. Since this relationship has an impact on the strains of the steel bar, it consequently affects the strain profile of the concrete as per Eqs. (32) and (33), and ultimately influences the crack-opening displacement through Eq. (39). Consequently, the bond stress-slip relationship is deeply intertwined with the crack-opening displacement, necessitating the adoption of an iterative algorithm to analyze this interaction and further elucidate the bond behavior of the cracked beam. The steps of the iterative algorithm are as follows:

1. Initiate the calculation process by giving initial reasonable values to the steel strain (ε_{sc0}) and to the slip (s_{p0} and s_{cc0}). Utilize these values to compute the coefficients α_0, f_{b0}, β_1, β_2, x_p, and c_3 in the bond stress-slip relationship using Eqs. (10), (13), and (18) – (21).
2. Determine the strain profiles in the concrete close to the cracks. Utilize ε_{sc0} to determine the parameters ε_{ct} and y_n within these profiles through Eqs. (32) and (33).
3. Utilize the parameters in the bond stress-slip relationship and the strain profiles to estimate the crack-opening displacement w_{cs} via Eq. (34), which is equated to the slip s_{ccr} at the crack. Subsequently, recalculate the slip s_{pr} at the intersection through Eq. (29).
4. Compare the last two calculated results of s_{cc} and s_p, and assess whether their difference falls within the acceptable limit defined by:

$$\left\|s_{pr} - s_{p0}\right\| + \left\|s_{ccr} - s_{cc0}\right\| < \gamma, \tag{40}$$

   where γ represents the allowable error and can be defined to be less than 5% of s_{pr}.
5. If Eq. (40) is valid, s_{ccr} and s_{pr} are established, enabling the determination of bond stresses based on the bond stress-slip relationship. Conversely, if Eq. (40) is not satisfied, evaluate the steel strain ε_{scr} using Eq. (30). Treat s_{ccr}, s_{pr} and ε_{scr} as the new initial values, and proceed with the calculation again, commencing from Step (2).

4. Experimental Validation

To validate the proposed approach, a comprehensive comparison is conducted between the theoretical results in this research project and some high-quality test results found in the literature (Brault and Hoult, 2019; Berrocal et al., 2021; Cantone et al., 2021), based on the use of fiber optic sensors to measure the strains in the bars; in this way, bond stresses could be very precisely evaluated by differentiating the steel strains.

4.1 Tests by Berrocal et al. (2021)

In these tests, RC beams were loaded in 4-point bending to determine the formation and location of cracks. These beams had a total length of 3,000 mm and a rectangular cross-section of 200 mm × 250 mm. One of the specimens, denoted as Beam 2, was explicitly described in the paper (Berrocal et al., 2021), and its properties were used to validate the proposed method. Beam 2 was reinforced with three bars at the bottom and two bars at the top, as shown in Fig. 3. The concrete compressive strength was 68.2 MPa. The diameters of the bottom and top bars were 16 mm and 10 mm, respectively.

The specimens were simply supported on rollers and loaded under 4-point bending, as shown in Fig. 3. The clear span between the center of the supports was equal to 2,700 mm. The loading procedure

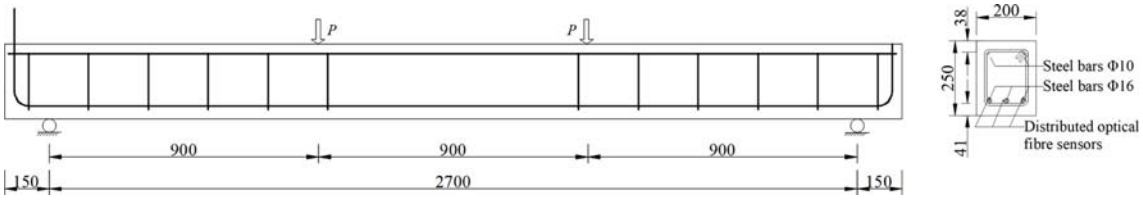

Fig. 3. Layout of the Beam Specimen Redrawn from the Literature (Berrocal et al., 2021) (unit: mm)

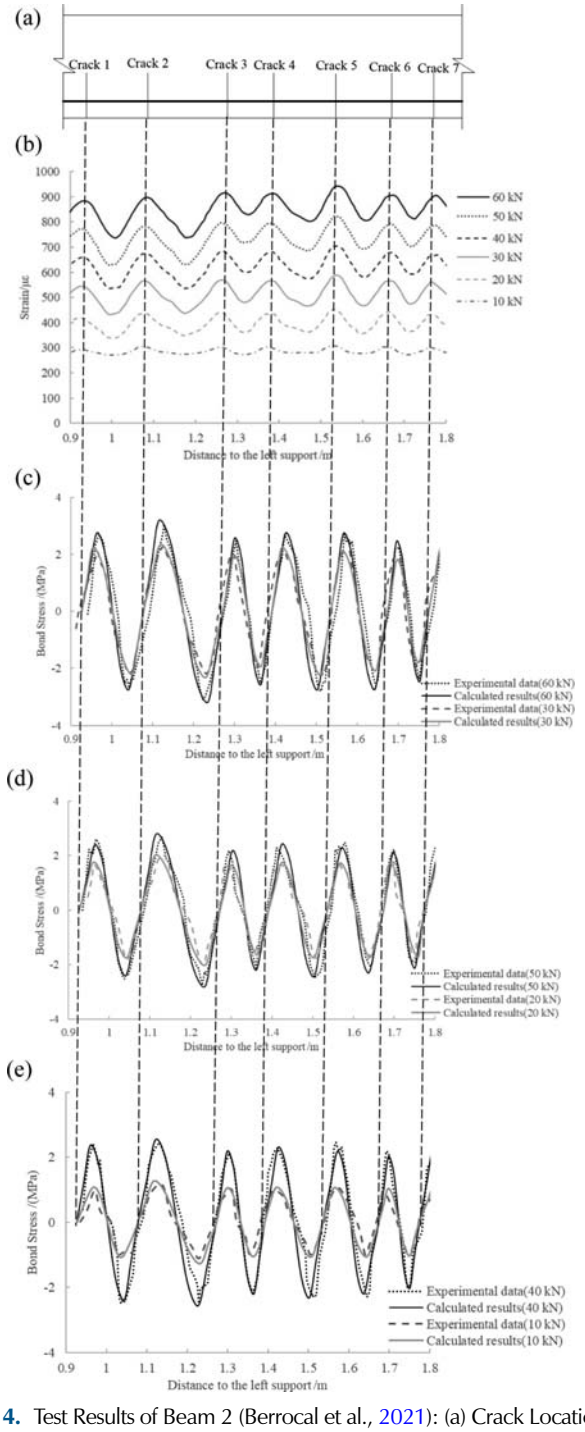

Fig. 4. Test Results of Beam 2 (Berrocal et al., 2021): (a) Crack Location, (b) Profiles of Steel Strains between the Two Points of Loading, (c) Profiles of Bond Stresses under the First Group of Loads, (d) Profiles of Bond Stresses under the Second Group, (e) Profiles of Bond Stresses under the Third Group

was displacement-controlled and the displacement rate was 0.5 mm/min. Two load cycles were performed, reaching a maximum total load of 60 kN and unloading down to 5 kN total load.

Optical fibers were glued on each of the bottom bars to record the steel strains. The strains of the bar on the left corner of the bottom during the load cycles are depicted in Fig. 4(a). A local maximum of the steel strains indicated the occurrence of a crack (Berrocal et al., 2021), based on which the crack locations were identified and illustrated in Fig. 3.

Once the strains have been measured, the bond stresses can be computed based on Eq. (6) and their results are depicted in three figures of Fig. 4. Based on the crack pattern, the bond stresses were also calculated using the proposed method, and the calculated and measured results were compared in Fig. 4. It is found that the calculated results agree very well with the test results, with reference to both the maximum values and the general trends. The proposed approach provides, therefore, a reliable tool to predict the bond stresses in RC beams exhibiting primary cracks. Note that the values of the bond stresses gradually decrease to zero in the cracked planes as a result of bond deterioration.

Figure 4 illustrates the maximum bond stresses are positively correlated with the applied load. Notably, the highest stress is observed at the load of 60 kN, whereas the lowest occurs under the load of 10 kN. Furthermore, the bond stresses exhibit an upward trend with increasing crack spacing. Under the load of 60 kN, the stresses attain their maximum between Cracks 2 and 3 thanks to the larger spacing of these cracks, while the stresses reach their minimum between Cracks 6 and 7 as a result of the smaller crack spacing. Conversely, the stresses between Cracks 3 and 4 closely approximate those between Cracks 6 and 7 due to their proximity in spacing. This trend persists similarly between Cracks 4 and 5 and between Cracks 5 and 6. The distribution characteristics of the bond stress under other loads mirror those under the load of 60 kN.

This behavior is attributed to the larger loads causing increased crack-opening displacements. Moreover, for a given load, cracks with wider spacings exhibit larger displacements, as depicted in Fig. 5. These larger displacements will cause bigger steel-concrete slip values, resulting in larger bond stresses. Similarly, cracks with close spacings exhibit correspondingly close bond stresses.

Once the slip and the bond stress have been evaluated, the bond stress-slip relationships in the region between Crack 2 and Crack 3 can be formulated, and their results are illustrated in Fig. 6. While the curved branches of these relationships are situated on the same curve under different loads, the linear branches show variations with loads. These linear branches originate at the points

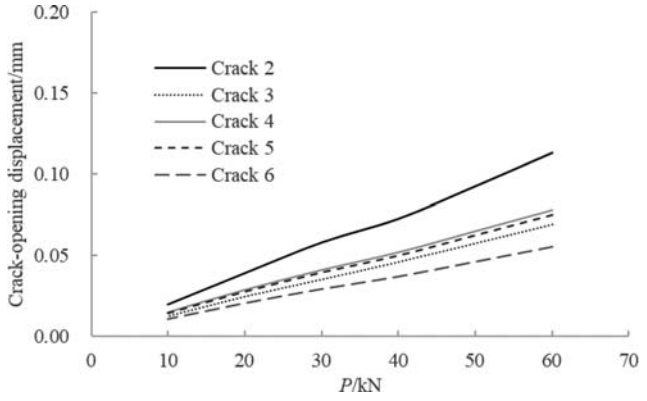

Fig. 5. Calculated Results of Crack-Opening Displacements at the Level of the Bar

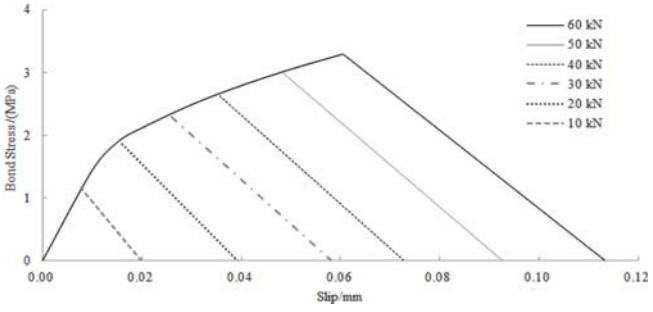

Fig. 6. Calculated Results of Bond Force–Slip Relationships in the Region between Cracks 2 and 3

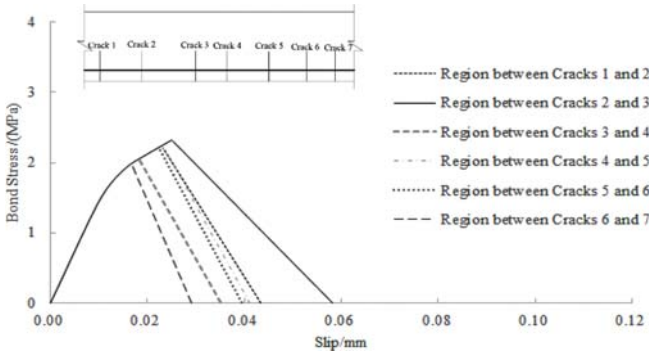

Fig. 7. Calculated Results of Bond Force–Slip Relationships in Different Regions under the Load of 30 kN

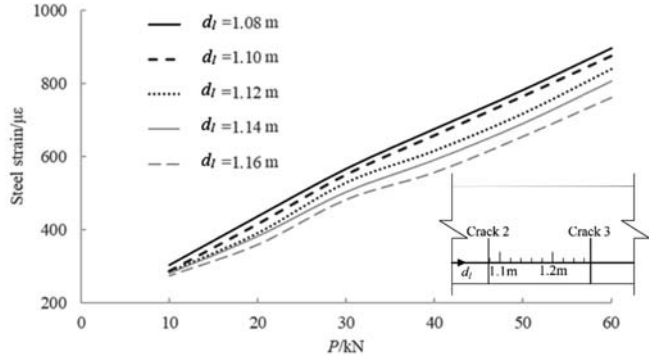

Fig. 8. Experimental Results of Steel Strains in the Different Positions (Berrocal et al., 2021)

where the bond stresses reach their peaks and terminate at the points where the slip values reach their local maximum, corresponding to the crack-opening displacements. Because of the evolution of crack-opening displacements under increasing loads, the linear branches are variable too. Furthermore, it is also observed from Fig. 6 that the peaks of the bond stresses increase nonlinearly with the loads, resulting in variations in the linear branches.

However, the linear branches of the relationships between Cracks 2 and 3 exhibit nearly constant slopes, regardless of applied loads, as depicted in Fig. 6. Therefore, if the relationship for a given region is known under a particular load, the linear branches of the relationships under other loads can be obtained by horizontally translating the known branch.

In Fig. 7, the bond stress-slip relationships for different regions are displayed, when the beam is subjected to the same load (30 kN). The linear branch of the relationship between Cracks 4 and 5 closely resembles that between Cracks 1 and 2, but it differs from that between Cracks 2 and 3. This is because the crack spacings in the former two regions are almost the same and differ from that in the latter region. A larger spacing corresponds to a bigger open displacement, leading to a different bond stress-slip relationship. Therefore, under the same load, the bond stress-slip relationships are affected by the crack pattern but remain almost the same in regions with the identical spacings.

As the bond stress-slip relationship varies with the crack-opening displacements and thus affects the displacements, the behavior of the RC beam exhibits nonlinear characteristics. The change in the strains of the bar near Crack 2 is shown in Fig. 8, where d_l represents the distance to the left support of the beam. It is observed that the strains increase linearly with the load for the positions close to Crack 2 (at a distance of 1.078 m from the left support). However, for the points further away from the crack, the strain profile exhibits a slight nonlinearity with the load.

This behavior arises from the smaller bond stress at points closer to the crack, compared to points further away where the bond stress becomes pronounced. In Fig. 6, it is illustrated that the peaks of bond stresses increase nonlinearly with the applied loads. Consequently, the steel strains demonstrate nonlinearity when the bond stress becomes pronounced, owing to the differential relationship between the bond stress and the steel strains outlined in Eq. (5). This nonlinearity also can be a manifestation of tension stiffening. As the bond stress increases, the tensile force transferred from the steel bar to the concrete grows, leading to a greater portion of the tensile force being borne by the concrete due to bending moments. Consequently, the steel bar retains a smaller portion, causing a reduction in the increase rate of the steel strains with the load.

4.2 Tests by Cantone et al. (2021), Brault and Hoult (2019)

Cantone et al. (2021), Brault and Hoult (2019) conducted experiments on RC beams to measure steel strains using embedded optical fibers. The beams tested by Cantone et al. (2021) were 3,000 mm long with a transverse section of 300 mm × 320 mm. The

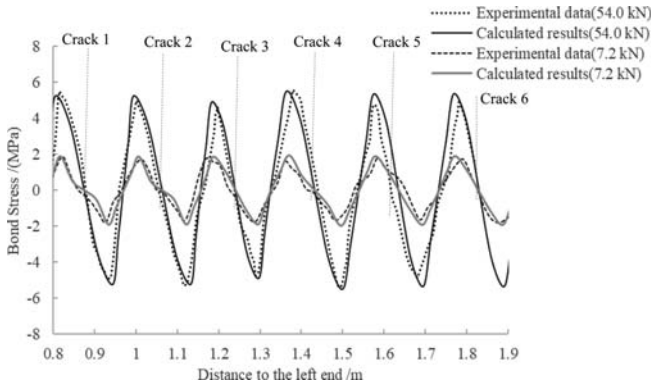

Fig. 9. Profiles of Bond Forces of SC76 (Cantone et al., 2021)

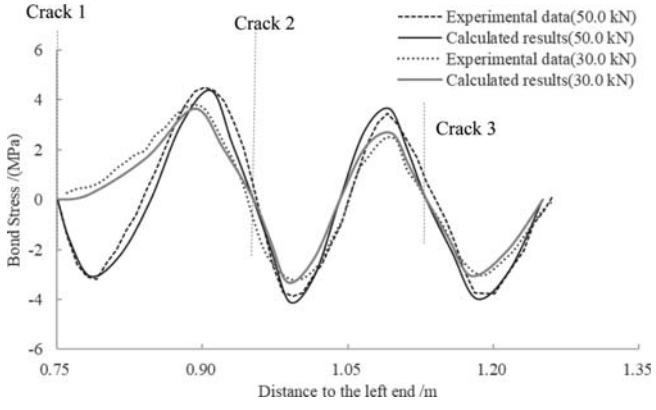

Fig. 10. Profiles of Bond Forces of LB2c (Brault and Hoult, 2019)

specimen, denoted as SC76, was considered in this study. The flexural reinforcement of the specimen consisted of two reinforcing bars at the bottom, with a diameter of 22 mm and a yield strength of 701 MPa. In the work by Brault and Hoult (2019), the specimen, denoted as LB2c, was considered. The span of the specimen is 2,000 mm, and the transverse sections were 300 mm × 200 mm rectangular sections. The longitudinal reinforcement bars near the bottom of the specimen were 15 mm-diameter ribbed bars, and the cracking patterns were recorded during loading.

Based on the measured strains, the bond stresses were obtained through Eq. (10), and also recalculated using the proposed method. The calculated and measured results were compared in Figs. 9 and 10. It is observed that these calculated results coincide with the data from both experiments.

In the experimental work by Brault and Hoult (2019), under the load of 30 kN, the bond stresses declined near every crack except for Crack 1. This is due to the fact that Crack 1 did not form under the load of 30 kN, and bar-concrete slip was, therefore, zero. Nevertheless, Crack 1 formed at the load of 50 kN and became visible, leading to a subsequent decrease in the bond stresses. Consequently, the bond stress profiles were greatly influenced by crack location and spacing.

5. Conclusions

Bond deterioration in RC beams close to primary cracks is investigated by means of a novel approach based on a bond stress-bar slip relationship whose parameters depend on the crack-opening displacement. Such a displacement is in turn evaluated based on the variable strain profiles in the concrete, through an iterative procedure. The effectiveness of the proposed approach is validated against a set of tests well documented in the literature, leading to the following conclusions:

1. The tests on RC beams confirm the efficacy of the proposed approach, revealing a decreasing trend in bond stresses near the cracks, starting from their maximum and eventually reaching zero. Furthermore, the peak of the bond stress depends on the crack pattern and on the applied load, both factors affecting the crack-opening displacement and – consequently– bond stresses.
2. The bond stress-slip relationship between two contiguous cracks is influenced by both the crack pattern and the applied loads, leading to variations in the maximum bond stress and slope of the relationship. Nevertheless, the bond-slip relationships display descending branches characterized by remarkably similar slopes within a given region, irrespective of the loads. Consequently, if the descending branch for this region is known under a particular load, the branches under other loads can be obtained by horizontally translating the known branch.
3. The strains in the steel bars are characterized by a nonlinear increase under increasing loads as a result of the nonlinear increase in the bond stresses and of the differential relationship between the stresses and the strains. Such nonlinearities are typical of the behavior of cracked RC beams.

Overall, the proposed approach provides valuable insights into the bond behaviors of cracked RC beams and offers an effective means of predicting bond stresses in different load conditions and for different crack patterns. These findings contribute to an improved understanding of the nonlinear behavior exhibited by RC beams in practical applications. Moreover, bond stresses determine the magnitude of tensile forces transferred from the steel bar to the concrete, thereby influencing the effect of tension stiffening, a critical factor impacting structural stiffness in the beams. By assessing bond stresses, the structural stiffness, as well as the stresses in the concrete can be evaluated, with possible contributions to structural design.

ORCID

Jianming Wang https://orcid.org/0009-0002-2788-6609
Jian Guo http://orcid.org/0000-0003-3605-2999
Chunyu Fu http://orcid.org/0000-0001-6865-9790

References

Balazs GL (1993) Cracking analysis based on slip and bond stresses. *ACI Materials Journal* 90(4):340-348, DOI: 10.14359/3890

Berrocal CG, Fernandez I, Bado MF, Casas JR, Rempling R (2021) Assessment and visualization of performance indicators of reinforced

concrete beams by distributed optical fiber sensing. *Structural Health Monitoring* 20(6):3309-3326, DOI: 10.1177/1475921720984431

Brault A, Hoult NA (2019) Distributed reinforcement strains: Measurement and application. *ACI Structural Journal* 116(4):115-127, DOI: 10.14359/51714483

Cairns J, Jones K (1996) An evaluation of the bond-splitting action of ribbed bars. *ACI Materials Journal* 93(1):10-19, DOI: 10.14359/9791

Cantone R, Ruiz MF, Muttoni A (2021) A detailed view on the rebar–to–concrete interaction based on refined measurement techniques. *Engineering Structures* 226:111332, DOI: 10.1016/j.engstruct.2020.111332

Castel A, Gilbert RI, Ranzi G (2014) Instantaneous stiffness of cracked reinforced concrete including steel-concrete interface damage and long-term effects. *Journal of Structural Engineering* 140(6):1-9, DOI: 10.1061/(ASCE)ST.1943-541X.0000954

Castel A, Vidal T, François R (2012) Finite-element modeling to calculate the overall stiffness of cracked reinforced concrete beams. *Journal of Structural Engineering* 138(8):889-898, DOI: 10.1061/(ASCE)ST.1943-541X.0000520

Debernard PG, Guiglia M, Taliano M (2013) Effect of secondary cracks for cracking analysis of reinforced concrete tie. *ACI Materials Journal* 110(2):209-216, DOI: 10.1007/s13296-013-1019-4

Debernard PG, Taliano M (2016) An improvement to Eurocode 2 and fib Model Code 2010 methods for calculating crack width in RC structures. *Structural Concrete* 17(3):365-376, DOI: 10.1002/suco.201500033

Fayyad TM, Lees JM (2018) Integrated fracture-based model formulation for RC crack analysis. *Journal of Structural Engineering* 144(7):04018083, DOI: 10.1061/(ASCE)ST.1943-541X.0002058

Fib (International Federation for Structural Concrete) (2000) fib Bulletin10. Bond of reinforcement in concrete: State-of-art report. fib, Lausanne, Switzerland

Fib (International Federation for Structural Concrete) (2013) Model Code for Concrete Structures 2010. Ernst & Sohn, Berlin, Germany

Fib (International Federation for Structural Concrete) (2014) fib Bulletin 72. Bond and anchorage of embedded reinforcement: Background to the fib Model Code for Concrete Structures 2010. fib, Lausanne, Switzerland

Fu C, Gao Z, Yan G (2022) Nonlinear steel strains in cracked RC beams based on bond stress profiles. *Materials and Structures* 55:209, DOI: 10.1617/s11527-022-02048-x

Fu C, Lao Y (2023) Steel–concrete bond deterioration in reinforced concrete tension members due to primary cracks. *Structures* 56:104895, DOI: 10.1016/j.istruc.2023.104895

Fu C, Zhu Y, Tong D (2021) Stiffness assessment of cracked reinforced concrete beams based on a fictitious crack model. *KSCE Journal of Civil Engineering* 25(2):516-528, DOI: 10.1007/s12205-020-2056-0

Gambarova PG, Rosati GP (1997) Bond and splitting in bar pull-out: Behavioural laws and concrete cover role. *Magazine of Concrete Research* 49(179):99-110, DOI: 10.1680/macr.1997.49.179.99

Gambarova PG, Rosati GP, Zasso B (1989) Steel-to-concrete bond after concrete splitting: Test results. *Materials and Structures* 22(1):35-47, DOI: 10.1007/BF02472693

Giuriani E, Plizzari GA (1998) Interrelation of splitting and flexural cracks in RC beams. *Journal of Structural Engineering* 124(9):1032-1040, DOI: 10.1061/(ASCE)0733-9445(1998)124:9(1032)

Hermawan H, Wiktor V, Gruyaert E, Serna P (2023) Experimental investigation on the bond behaviour of steel reinforcement in self-healing concrete. *Construction and Building Materials* 383:131378, DOI: 10.1016/j.conbuildmat.2023.131378

Jakubovskis R, Kaklauskas G (2019) Bond–stress and bar–strain profiles in RC tension members modelled via finite elements. *Engineering Structures* 194:138-146, DOI: 10.1016/j.engstruct.2019.05.069

Jakubovskis R, Kaklauskas G (2021) Damage of bond in reinforced concrete: A detailed finite element analysis. *Structural Concrete* 22:3228-3240, DOI: 10.1002/suco.202100229

Kaklauskas G (2017) Crack model for RC members based on compatibility of stress–transfer and mean–strain approaches. *Journal of Structural Engineering* 143:04017105, DOI: 10.1061/(ASCE)ST.1943-541X.0001842

Marfia S, Rinaldi Z, Sacco E (2004) Softening behaviour of reinforced concrete beams under cyclic loading. *International Journal of Solids and Structures* 41:3293-3316, DOI: 10.1016/j.ijsolstr.2003.12.015

Mousavi SS, Guizani L, Ouellet-Plamondon CM (2019) On bond-slip response and development length of steel bars in pre-cracked concrete. *Construction and Building Materials* 199:560-573, DOI: 10.1016/j.conbuildmat.2018.12.039

Muhamad R, Ali MSM, Oehlers DJ, Griffith M (2012) The tension stiffening mechanism in reinforced concrete prisms. *Advances in Structural Engineering* 15:2053-2069, DOI: 10.1260/1369-4332.15.12.2053

Murray A, Gilbert RI, Castel A (2018) A new approach to modeling tension stiffening in reinforced concrete. *ACI Structural Journal* 115(1):127-137, DOI: 10.14359/51700952

Parvanova S, Gospodinov G (2008) Development of "event–to–event" nonlinear technique to lightly reinforced concrete beams by simplified constitutive modeling. *International Journal of Solids and Structures* 45:4676-4686, DOI: 10.1016/j.ijsolstr.2008.04.005

Rabczuk T, Akkermann J, Eibl J (2005) A numerical model for reinforced concrete structures. *International Journal of Solids and Structures* 42:1327-1354, DOI: 10.1016/j.ijsolstr.2004.07.019

Ruiz G (2001) Propagation of a cohesive crack crossing a reinforcement layer. *International Journal of Fracture* 111:265-282, DOI: 10.1023/A:1012260410704

Ruiz MF, Muttoni A, Gambarova PG (2007) Analytical modeling of the pre–and postyield behaviour of bond in reinforced concrete. *Journal of Structural Engineering* 133:1364-1372, DOI: 10.1061/(ASCE)0733-9445(2007)133:10(1364)

Somma G, Vit M, Frappa G, Pauletta M, Pitacco I, Russo G (2021) A new cracking model for concrete ties reinforced with bars having different diameters and bond laws. *Engineering Structures* 235:112026, DOI: 10.1016/j.engstruct.2021.112026

Taliano M (2017) Cracking analysis of concrete tie reinforced with two diameter bars accounting for the effect of secondary cracks. *Engineering Structures* 144:107-119, DOI: 10.1016/j.engstruct.2017.04.045

Tan R, Hendriks MAN, Geiker M, Kanstad T (2020) A numerical investigation of the cracking behaviour of reinforced–concrete tie elements. *Magazine of Concrete Research* 72(3):109-121, DOI: 10.1680/jmacr.18.00156

Wu HQ, Gilbert RI (2009) Modeling short–term tension stiffening in reinforced concrete prisms using a continuum–based finite element model. *Engineering Structures* 31(10):2380-2391, DOI: 10.1016/j.engstruct.2009.05.012

Xu T, Zhu L, Castel A, Gilbert RI (2018) Assessing immediate and time-dependent instantaneous stiffness of cracked reinforced concrete beams using residual cracks. *Journal of Structural Engineering* 144(4):1-12, DOI: 10.1061/(ASCE)ST.1943-541X.0002009

Yankelevsky DZ, Jabareen M, Abutbul AD (2008) One–dimensional analysis of tension stiffening in reinforced concrete with discrete cracks. *Engineering Structures* 30(1):206-217, DOI: 10.1016/j.engstruct.2007.03.013